

Ultrasensitive Tip- and Antenna-Enhanced Infrared Nanoscopy of Protein Complexes

Brian T. O’Callahan,[†] Mario Hentschel,[‡] Markus B. Raschke,[§] Patrick Z. El-Khoury,[†] and A. Scott Lea^{*,†}

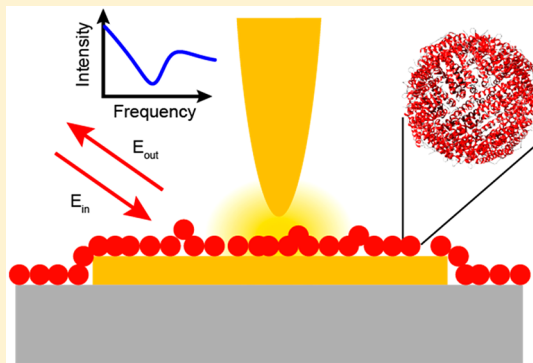
[†]Environmental Molecular Sciences Laboratory, Pacific Northwest National Laboratory, Richland, Washington 99352, United States

[‡]4th Physics Institute, Research Center SCoPE, and Center for Integrated Quantum Optics, IQST University of Stuttgart, Pfaffenwaldring 57, 70569 Stuttgart, Germany

[§]Department of Physics, Department of Chemistry, and JILA, University of Colorado at Boulder, Boulder, Colorado 80309, United States

Supporting Information

ABSTRACT: Surface-enhanced infrared absorption (SEIRA) using resonant plasmonic nanoantennas enables zeptomolar detection sensitivity of (bio)analytes, although with diffraction limited spatial resolution. In contrast, infrared scattering–scanning near-field optical microscopy (IR *s*-SNOM) allows simultaneous imaging and spectroscopy with nanometer spatial resolution through vibrational coupling to the antenna mode of a probe tip. Herein, we combine these two approaches to image distributions of ferritin protein complexes adsorbed onto IR-resonant Au nanoantennas. The joint tip and antenna enhancement yields single protein complex sensitivity due to coupling with the vibrational modes of the bioanalytes. The coupling is revealed through IR *s*-SNOM spectra in the form of Fano line shapes, which can be modeled by using coupled harmonic oscillators. The role of the antenna resonance frequency on the coupling strength and the sensitivity is explored. Inhomogeneities in protein density within the film can be detected at single protein complex level. This work paves the way for single protein identification and imaging through a combination of tip- and antenna-enhanced IR nanoscopy.



1. INTRODUCTION

Single protein chemical imaging and identification has remained an ultimate goal of analytical biology. Recent surface-enhanced infrared absorption (SEIRA) and surface-enhanced Raman spectroscopy (SERS) studies exploited the interactions between molecular vibrations and enhanced electromagnetic fields associated with surface plasmons to significantly improve the detection limit in (bio)analytical vibrational spectroscopy.^{1–3} Of particular relevance to this work are recent implementations of SEIRA using nano-fabricated antennas, whereby modes that are resonant with typical IR vibrational frequencies dramatically improve SEIRA sensitivity to few-nanometer-thick protein monolayers.^{4–6} Even sensitivity to tens of zeptomoles of proteins has been demonstrated by using the aforementioned spectroscopic approach.⁷ Overall, such tailored structures with their well-controlled plasmonic properties provide an invaluable platform for *in situ* (bio)chemical identification and structural analysis through infrared spectroscopy.^{8,9}

Tip-enhanced infrared spectroscopy allows similar analyses to be performed, but now with additional nanometer spatial resolution. This is achieved through large wavevector

components of localized optical fields in the vicinity of the apex of a sharp metallic scanning probe tip that both mode match far-field light to molecular vibrational modes as well as enable nanoscale spatial resolution.¹⁰ In scattering-type scanning near-field optical microscopy (*s*-SNOM), infrared light illuminates the tip, which then locally probes the chemical identity of (bio)molecules with high sensitivity and nanometer spatial resolution.^{11–15} In the realm of biosensing, recent IR *s*-SNOM studies have directly demonstrated single protein complex sensitivity and even inferred the ultimate detection limit of a single protein.^{11,12} However, past studies relied solely on tip enhancement, with very few demonstrations of combined *s*-SNOM-SEIRA schemes^{16,17} to image nonbiological analytes.

Herein, we combine tip- and antenna-enhanced IR nanospectroscopy with the ultimate goal of identifying and imaging nanoscopic protein complexes. Specifically, we interrogate a coupled ferritin complex–antenna system (see Figure 1) with

Received: June 17, 2019

Revised: June 25, 2019

Published: June 25, 2019

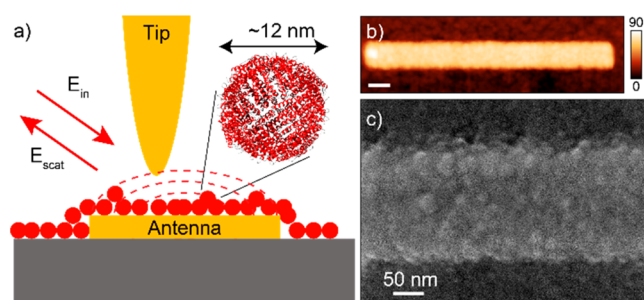


Figure 1. Experimental schematic and sample characterization. (a) An IR nanoantenna with close to monolayer protein coverage is excited with the incident field, E_{in} , and probed with a Au-coated AFM tip. The scattered field, E_{scat} , reflects the local vibrational properties of the biomolecules. The inset of (a) shows the ferritin, which consists of 24 protein subunits that are predominantly composed of α -helices (PDB: 1MFR). (b) High-resolution AFM image (scale bar: 200 nm) and (c) He ion micrograph showing the distribution of ferritin units across the antenna.

single protein complex sensitivity. Through signal-to-noise analysis, we demonstrate a 3 orders of magnitude sensitivity improvement over past SEIRA demonstrations as well as an order of magnitude sensitivity improvement over conventional *s*-SNOM measurements with unpatterned substrates, which we achieve through the coupling of the protein and antenna modes. The tip/antenna coupling is revealed in the IR *s*-SNOM spectra in the form of Fano line shapes. Fits to a coupled harmonic oscillator model enable extraction of the antenna–vibrational mode coupling strengths as well as the vibrational peak frequencies and line widths that report on the chemical compositions and conformations of our bioanalyte. Our results thus pave the way for single protein identification and conformational analysis.

2. METHODS

The substrate used in this study consists of nanofabricated gold nanorods atop a CaF_2 substrate (Figure 1a). The antennas are fabricated with standard electron beam lithography (Raith eLine) in double-layer poly(methyl methacrylate) resist (200 and 950 K, Allresist). A 4 nm titanium adhesion layer and a 70 nm gold layer are electron beam evaporated, followed by lift-off. The width of the antennas is 200 nm, and their length ranges from 1.7 to 2.3 μm . A thin layer of ferritin proteins

(Sigma-Aldrich, PN: F4503) was deposited onto the sample by spin-coating 10 μL of an aqueous 12 μM protein solution at 3000 rpm for 20 s. Ferritin is a 474 kDa protein complex composed of 24 subunits with predominantly α -helical secondary structure. High-resolution atomic force microscopy (AFM) (Figure 1b) and helium-ion microscopy (HIM) (Figure 1c) together confirm continuous monolayer surface coverage with the ~ 12 nm diameter protein complexes, with occasional bilayer regions. Larger scale morphology is due to roughness in the underlying gold antenna, which we characterize through HIM. The nanorod acts as a half-wavelength antenna with its plasmonic resonance in the amide I spectral region.¹⁰ We excite this plasmonic antenna mode with focused light from a quantum cascade laser (MIRcat, Daylight solutions) polarized along the long axis of the nanorod. The resulting evanescent field encompasses the ferritin layer and allows coupling between the antenna and protein resonances. Far-field transmission spectra of the coated antenna were obtained using a commercial FTIR microscope (IFS 66/s, Bruker) with a 15 \times 0.4 NA objective.

The local field enhancement and mode coupling underlies the improved sensitivity of SEIRA.^{1–3} By use of *s*-SNOM, a sharp metallized probe tip of an AFM (attoAFM II, Attocube) operating in intermittent contact mode further improves sensitivity through localizing fields at the tip apex and simultaneously scattering the evanescent fields into far-field radiation.^{11,12,14,18} The tip-scattered light, which reflects the local IR vibrational response, was collected with an off-axis parabolic mirror and detected with a mercury–cadmium–telluride detector (KLD-0.25-J1/11/DC5M, Kolmar Technologies).¹³ We interfered the scattered field with light from a reference arm and extracted the complex-valued near-field signal using a pseudo-heterodyne demodulation technique.¹⁹ High-resolution AFM was performed using an uncoated Si tip with typical apex radius of curvature $r \approx 2$ nm (SSS-NCHR, Nanosensors) using intermittent contact AFM feedback. Helium ion images were acquired using a commercial microscope (Orion Plus, Zeiss) operating at 30 kV and 0.9 pA.

3. RESULTS

Figure 2 shows the simultaneously acquired AFM topography (a) and near-field image (b) of a ferritin-coated nanorod with an antenna resonance that is tuned to the amide I frequency

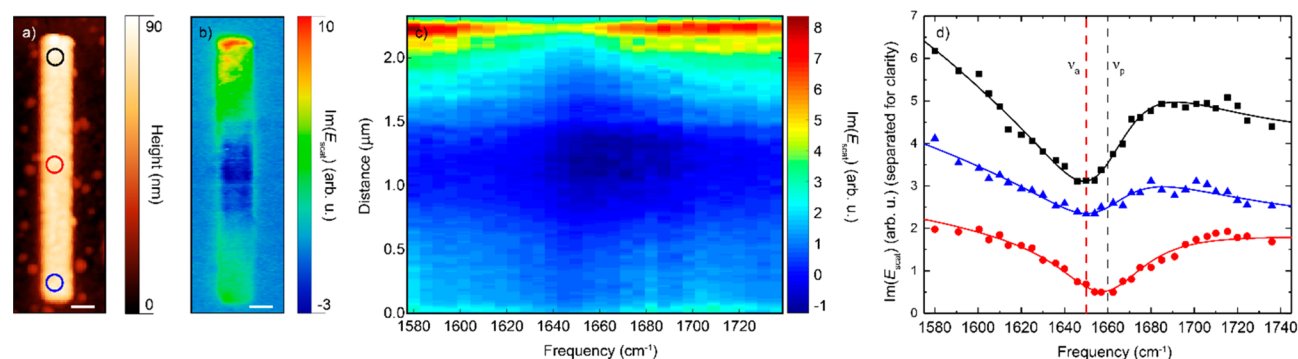


Figure 2. Spatiospectral IR *s*-SNOM imaging and spectroscopy of protein coupled to a resonant antenna of length $L = 2.0 \mu\text{m}$ with resonant frequency 1650 cm^{-1} . (a) Topography of ferritin-coated nanorod and (b) corresponding near-field map at $\bar{\nu} = 1662.5 \text{ cm}^{-1}$. Scale bar is 200 nm. Fano line shapes are observed in (c) spatially resolved spectra extracted along the antenna length and (d) point spectra from points indicated in (a). The blue curve is offset by $\text{Im}(E_{scat}) = 1$ for clarity. The red and black dashed lines indicate the resonance frequency of the antenna $\bar{\nu}_a$ and the protein amide I response $\bar{\nu}_{p,I}$, respectively.

($\bar{\nu}_0 \approx 1650 \text{ cm}^{-1}$) and a bandwidth that adequately covers the amide I and II bands (fwhm = 500 cm^{-1}). Because of tip convolution and the ferritin layer, the antenna appear slightly longer than the stated lengths. The near-field image is dominated by the electric field spatial profile of the antenna dipole mode as expected, with small spatial variations due to the inhomogeneity in protein film thickness. The spatial field profile of the antenna deviates from that of an ideal half-wavelength antenna due to a strong contribution from Au-tip excitation.²⁰ A series of 30 images at distinct excitation wavelengths ($\Delta\bar{\nu} \approx 5 \text{ cm}^{-1}$ step size in the $\sim 1580\text{--}1735 \text{ cm}^{-1}$ range) were recorded and together comprise a spatio-spectral data set or hyperspectral image cube. Each image was normalized to a subregion of the image on the bare ferritin/CaF₂ surface, which has negligible vibrational signature (see the Supporting Information). Our study focused on the amide I spectral region due to its role in identifying secondary structure of proteins.

Figure 2c,d shows a line scan taken along the long axis of the antenna and representative point spectra extracted from regions of interest indicated in Figure 2a. These spectra exhibit asymmetric, dispersive line shapes toward either end of the nanorod and a symmetric dip in the center. To fit our spectra, we apply a two coupled harmonic oscillator model similar to that developed by Muller et al.¹⁶ This model treats the spectral responses g_i of the polarization of the antenna and the vibrational modes as Lorentzian functions:

$$g_i(\bar{\nu}) = -\bar{\nu}^2 + \bar{\nu}_i^2 - i\bar{\nu}\Delta\bar{\nu}_i - k \quad (1)$$

where $\bar{\nu}_i$ and $\Delta\bar{\nu}_i$ correspond to the resonance frequencies and line widths, and k designates the coupling strength between the vibrational and antenna resonances. The tip-scattered field \tilde{E}_{scat} is then given by

$$\tilde{E}_{\text{scat}} \propto \sum_i a_i \frac{\tilde{E}_v k - \tilde{E}_a g_{v,i}}{g_{v,i} g_a - k_i^2} \quad (2)$$

where \tilde{E}_a and \tilde{E}_v are the complex field amplitudes of the antenna and the vibrational mode, respectively, and the sum is over the vibrational modes of the protein. Here, we include both the amide I and amide II resonances around $\bar{\nu}_{v,I} = 1660 \text{ cm}^{-1}$ and $\bar{\nu}_{v,II} = 1540 \text{ cm}^{-1}$ as separate Lorentzian oscillators. Note that although the vibrational response of the protein should formally be described by Gaussian profiles, we find that a sum of two Lorentzian profiles results in a good approximation to the measured line shape. In general, a Gaussian line shape could be constructed via eq 2 by summing over a distribution of such Lorentzian functions with the corresponding distribution function for $a_i(\bar{\nu})$.

Fits to the two oscillator model reproduce the experimental traces, as shown in Figure 2d, with a protein amide I peak frequency $\bar{\nu}_{v,I} = 1660 \text{ cm}^{-1}$ and a line width $\Delta\bar{\nu}_{v,I} = 56 \text{ cm}^{-1}$. Both of these values match the IR vibrational response of α -helix secondary structures within our $\sim 5 \text{ cm}^{-1}$ spectral resolution.^{11,12,21}

We tune the antenna resonance frequency by varying the nanorod length. Figure 3a shows the s-SNOM spectra of ferritin-coated nanorods with different lengths L , acquired on the antenna terminal with highest field magnitude. The shift in resonance frequency is evident in the far-field transmission spectra shown in Figure 3b. The molecular signature as measured by the depth of the Fano profile is maximized when

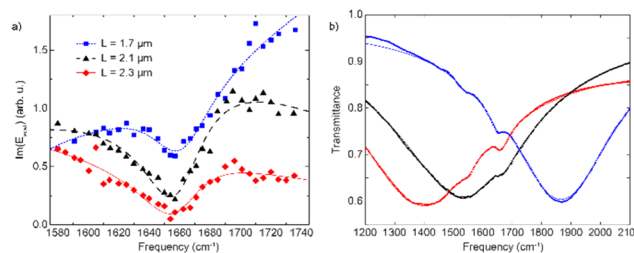


Figure 3. Effect of antenna resonant frequency on the vibrational signal enhancement. (a) s-SNOM spectra as a function of antenna length L . Detuned antenna resonances result in more asymmetric spectra and weaker molecular response. (b) Corresponding far-field transmittance spectra of the coated antennas showing the plasmonic resonance frequencies.

the antenna resonance is tuned to the vibrational frequency (black curve). For the detuned cases (blue and red), the spectra show a weaker vibrational response and additionally a higher degree of asymmetry.

4. DISCUSSION

The coupling strength k governs the magnitude of the molecular signal enhancement through the IR antenna excitation. While in general the coupling strength to the amide I and the amide II resonances may differ, the fits in Figure 2d use the same k value for both resonances since the antenna response varies by <10% between the amide I and amide II spectral regions. For our system, we find that the spectra are fit well with $k = 17, 13,$ and 9 cm^{-1} for the lower, middle, and top terminals of the rod, respectively. Strong coupling, which is defined by the relation $C = \frac{|k|}{|\Delta\bar{\nu}_v + \Delta\bar{\nu}_a|} \gtrsim 0.25$,²² occurs when the coupling rate exceeds the natural line widths, and the vibrational mode and the antenna mode can no longer be considered separate emitters.¹⁶ Given our typical coupling strengths of $k \sim 10\text{--}20 \text{ cm}^{-1}$, we have $C \approx 0.03$, which establishes this system in the weak coupling regime. The low value of C is in part due to the relatively large spectral line width within proteins due to high inhomogeneous broadening. To move to the strong coupling regime, it is critical to reduce $\Delta\bar{\nu}_a$, which has recently been achieved by implementing a ground plane geometry that reduces the antenna resonance line width,¹⁶ or through coupling to narrow-band phonon polaritons as in the case of hexagonal boron nitride.¹⁷ An additional hurdle for strong coupling in this protein–antenna system is the large mode mismatch between the vibrational mode and the collective plasmon mode. While the sharp apex of the tip in part overcomes this spatial mismatch, further improvements of the antenna design can be implemented, including the use of, for example, gap-mode antennas which provide even higher optical field confinement.²³

We now further analyze the sensitivity of our spatio-spectral maps. Figures 4a and 4b are selected area topographic and optical nanographs, respectively. The topographic image shows a small, $\sim 10 \text{ nm}$ high feature near the end of the nanorod. The location of the peaked optical contrast is slightly offset from the topography data due to the nonuniform field at the edge of the antenna.²⁴ While its height is consistent with a single ferritin complex, its lateral dimension is determined by convolution with the AFM tip radius. Notice that this topographic feature is correlated to a factor of ~ 2 change in

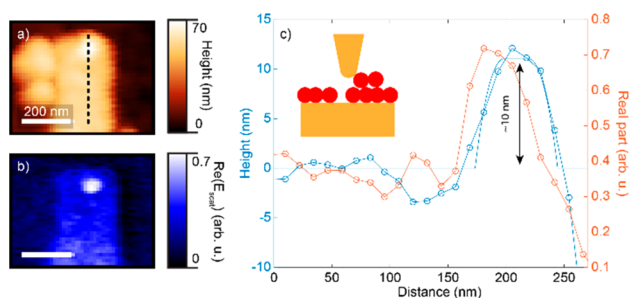


Figure 4. (a) Topography and (b) near-field image acquired at $\bar{\nu} = 1671 \text{ cm}^{-1}$ of the upper terminal region of an antenna with a small protein aggregate (antenna length $L = 2.1 \mu\text{m}$). (c) Line cuts taken along the dashed line in (a). Topography indicates a 10 nm high feature, corresponding to the diameter of the ferritin complex, is correlated to a factor of ~ 2 increase in optical signal. The solid blue line is a fit of the topography line cut to a tip-scan model used to extract the deconvoluted aggregate dimensions.

s-SNOM signal (Figure 4c), matching the expected signal increase due to an additional ferritin complex layer residing on the monolayer surface.

To estimate the actual dimension of this ferritin aggregate, we use a tip-scan model to deconvolute the topography line cut from the physical shape of the tip (see the Supporting Information for details). By fitting the model to a line cut along the sharp antenna edge, we extract a tip radius of $r = 50 \text{ nm}$, and using this value we determine that the lateral extent of the aggregate is $\sim 25 \text{ nm}$, corresponding to two ferritin diameters. This implies that the aggregate consists of ~ 7 ferritin complexes assuming a hexagonal close-packed configuration. The contrast between the aggregate and the monolayer region is $\Delta \text{Re}(E_{\text{scat}}) \simeq 0.4$ and is imaged with a corresponding SNR ~ 20 (RMS noise level on the substrate is $\text{RMS}(\text{Re}(E_{\text{scat}})) \simeq 0.02$), which indicates that single protein complex sensitivity can be achieved with SNR ~ 2.9 in single frequency spatial imaging. While single protein complex sensitivity has previously been demonstrated for an isolated complex,¹¹ our results indicate that inhomogeneities in protein density within aggregates and thin films can be imaged with single protein complex sensitivity, or ~ 20 – 30 individual protein sensitivity.

The resolution of an ~ 7 ferritin complex aggregate corresponds to $\sim 0.01 \text{ zmol}$ sensitivity of the 474 kDa protein complex, corresponding to a total protein mass of $3 \times 10^3 \text{ kDa}$. Recent SEIRA studies using similar nanorods as nanoantennas routinely demonstrate monolayer sensitivity.^{3,5,6} Using an array of nanoantennas, Adato et al.⁷ demonstrated a detection limit of down to 300 zmol of silk fibroin (molecular mass $M = 375 \text{ kDa}$), which corresponds to $6 \times 10^7 \text{ kDa}$ of protein. However, more sophisticated antenna structures have improved this limit by up to an order of magnitude.²⁵ Our results thereby represent a 3 orders of magnitude improvement of sensitivity over the state-of-the-art SEIRA studies and a 4 orders of magnitude improvement of sensitivity over conventional nanorod-based measurements.

We estimate spectral noise by calculating the RMS deviation of ~ 100 independent spectral measurements within the data set in Figure 2 from their collective average and obtain a SNR of 10. To compare spectral sensitivity across varying experimental conditions, we calculate the normalized signal-to-noise ratio (NSNR) given by $\text{NSNR} = \text{SNR}/(t^{1/2}\delta\nu)$ for acquisition time t and spectral resolution $\delta\nu$. Our acquisition time is given by our pixel dwell time multiplied by the number

of scans $t = 10 \text{ ms} \times 30 \text{ scans} = 300 \text{ ms}$, and our spectral resolution is $\delta\nu = 5 \text{ cm}^{-1}$. Our $\text{NSNR} = 7.6 \sqrt{\text{Hz}}/\text{cm}^{-1}$ is consistent with previous *s*-SNOM spectroscopic studies.²⁶ For comparison, we also analyzed a ferritin sample spin-coated onto a uniform, unpatterned Au surface (see the Supporting Information) and obtained $\text{NSNR} = 0.63 \sqrt{\text{Hz}}/\text{cm}^{-1}$ on an $\sim 40 \text{ nm}$ thick region. Comparison of the NSNR values normalized by the respective sample thicknesses indicates that our sensitivity is enhanced by an order of magnitude due to the resonant signal enhancement provided by the nanoantenna.

5. CONCLUSIONS

Combining antenna-enhanced SEIRA and tip-enhanced nano-spectroscopy, we demonstrate high sensitivity to protein vibrational signatures down to the few protein limit. This sensitivity relies on resonant coupling between the vibrational polarization and plasmonic fields of the antenna and boasts a 3 orders of magnitude sensitivity improvement over far-field resonant SEIRA studies. Our experimental spectra are well described by a coupled harmonic oscillator model, with coupling strengths $k \simeq 17 \text{ cm}^{-1}$, establishing this system in the weak coupling regime. Improvements to coupling strength and, in turn, sensitivity could be achieved by reducing antenna line width through either incorporating a ground-plane geometry or by coupling to narrow-band phonon polaritons. Overall, this work paves the way for single protein identification and conformational analysis through the combination of IR *s*-SNOM and SEIRA.

■ ASSOCIATED CONTENT

Supporting Information

The Supporting Information is available free of charge on the ACS Publications website at DOI: 10.1021/acs.jpcc.9b05777.

A spectrum ferritin on a uniform gold surface and model dependence on the coupling strength and the phase of the molecular field (PDF)

■ AUTHOR INFORMATION

Corresponding Author

*(A.S.L.) E-mail scott.lea@pnnl.gov.

ORCID

Brian T. O'Callahan: 0000-0001-9835-3207

Mario Hentschel: 0000-0002-6882-4183

Markus B. Raschke: 0000-0003-2822-851X

Patrick Z. El-Khoury: 0000-0002-6032-9006

Notes

The authors declare no competing financial interest.

■ ACKNOWLEDGMENTS

A.S.L., B.T.O., M.B.R., and P.Z.E. are supported by the Department of Energy (DOE), Office of Science, Biological and Environmental Research (BER) Bioimaging Technology project # 69212. M.B.R. also acknowledges STROBE, a National Science Foundation Science and Technology Center (Grant DMR 1548924). M.H. acknowledges funding from ERC (Complexplas), MWK Baden-Württemberg (ZAQuant, IQST), DFG (SPP1839), and BW Stiftung (Proteinsens). This work was performed in the Environmental Molecular Sciences Laboratory (EMSL), a DOE Office of Science User Facility sponsored by BER and located at Pacific Northwest National

Laboratory (PNNL). PNNL is operated by Battelle Memorial Institute for the DOE under Contract DE-AC05-76RL1830.

REFERENCES

- (1) Han, X. X.; Zhao, B.; Ozaki, Y. Surface-enhanced Raman Scattering for Protein Detection. *Anal. Bioanal. Chem.* **2009**, *394*, 1719–1727.
- (2) Bantz, K. C.; Meyer, A. F.; Wittenberg, N. J.; Im, H.; Kurtuluş, Ö.; Lee, S. H.; Lindquist, N. C.; Oh, S.-H.; Haynes, C. L. Recent Progress in SERS Biosensing. *Phys. Chem. Chem. Phys.* **2011**, *13*, 11551–11567.
- (3) Ataka, K.; Stripp, S. T.; Heberle, J. Surface-enhanced Infrared Absorption Spectroscopy (SEIRAS) to Probe Monolayers of Membrane Proteins. *Biochim. Biophys. Acta, Biomembr.* **2013**, *1828*, 2283–2293.
- (4) Cetin, A. E.; Etezadi, D.; Altug, H. Accessible Nearfields by Nanoantennas on Nanopedestals for Ultrasensitive Vibrational Spectroscopy. *Adv. Opt. Mater.* **2014**, *2*, 866–872.
- (5) Aksu, S.; Cetin, A. E.; Adato, R.; Altug, H. Plasmonically Enhanced Vibrational Biospectroscopy Using Low-Cost Infrared Antenna Arrays by Nanostencil Lithography. *Adv. Opt. Mater.* **2013**, *1*, 798–803.
- (6) Wu, C.; Khanikaev, A. B.; Adato, R.; Arju, N.; Yanik, A. A.; Altug, H.; Shvets, G. Fano-resonant Asymmetric Metamaterials for Ultrasensitive Spectroscopy and Identification of Molecular Monolayers. *Nat. Mater.* **2012**, *11*, 69–75.
- (7) Adato, R.; Yanik, A. A.; Amsden, J. J.; Kaplan, D. L.; Omenetto, F. G.; Hong, M. K.; Erramilli, S.; Altug, H. Ultra-Sensitive Vibrational Spectroscopy of Protein Monolayers with Plasmonic Nanoantenna Arrays. *Proc. Natl. Acad. Sci. U. S. A.* **2009**, *106*, 19227–19232.
- (8) Semenishyn, R.; Hentschel, M.; Stanglmair, C.; Teutsch, T.; Tarin, C.; Pacholski, C.; Giessen, H.; Neubrech, F. In Vitro Monitoring Conformational Changes of Polypeptide Monolayers Using Infrared Plasmonic Nanoantennas. *Nano Lett.* **2019**, *19*, 1–7.
- (9) Etezadi, D.; Warner, J. B.; Lashuel, H. A.; Altug, H. Real-Time In Situ Secondary Structure Analysis of Protein Monolayer with Mid-Infrared Plasmonic Nanoantennas. *ACS Sens.* **2018**, *3*, 1109–1117.
- (10) Olmon, R. L.; Krenz, P. M.; Jones, A. C.; Boreman, G. D.; Raschke, M. B. Near-field Imaging of Optical Antenna Modes in the Mid-infrared. *Opt. Express* **2008**, *16*, 20295–20305.
- (11) Amenabar, I.; et al. Structural Analysis and Mapping of Individual Protein Complexes by Infrared Nanospectroscopy. *Nat. Commun.* **2013**, *4*, 2890.
- (12) Berweger, S.; Nguyen, D. M.; Muller, E. A.; Bechtel, H. A.; Perkins, T. T.; Raschke, M. B. Nano-Chemical Infrared Imaging of Membrane Proteins in Lipid Bilayers. *J. Am. Chem. Soc.* **2013**, *135*, 18292–18295.
- (13) O'Callahan, B. T.; Crampton, K. T.; Novikova, I. V.; Jian, T.; Chen, C.-L.; Evans, J. E.; Raschke, M. B.; El-Khoury, P. Z.; Lea, A. S. Imaging Nanoscale Heterogeneity in Ultrathin Biomimetic and Biological Crystals. *J. Phys. Chem. C* **2018**, *122*, 24891–24895.
- (14) Paulite, M.; Fakhraei, Z.; Li, I. T. S.; Gunari, N.; Tanur, A. E.; Walker, G. C. Imaging Secondary Structure of Individual Amyloid Fibrils of a β 2-Microglobulin Fragment Using Near-Field Infrared Spectroscopy. *J. Am. Chem. Soc.* **2011**, *133*, 7376–7383.
- (15) Brehm, M.; Taubner, T.; Hillenbrand, R.; Keilmann, F. Infrared Spectroscopic Mapping of Single Nanoparticles and Viruses at Nanoscale Resolution. *Nano Lett.* **2006**, *6*, 1307–1310.
- (16) Muller, E. A.; Pollard, B.; Bechtel, H. A.; Adato, R.; Etezadi, D.; Altug, H.; Raschke, M. B. Nanoimaging and Control of Molecular Vibrations through Electromagnetically Induced Scattering Reaching the Strong Coupling Regime. *ACS Photonics* **2018**, *5*, 3594–3600.
- (17) Autore, M.; et al. Boron Nitride Nanoresonators for Phonon-enhanced Molecular Vibrational Spectroscopy at the Strong Coupling Limit. *Light: Sci. Appl.* **2018**, *7*, 17172.
- (18) Raschke, M. B.; Lienau, C. Apertureless Near-field Optical Microscopy: Tip-sample Coupling in Elastic Light Scattering. *Appl. Phys. Lett.* **2003**, *83*, 5089–5091.
- (19) Ocelic, N.; Huber, A.; Hillenbrand, R. Pseudoheterodyne Detection for Background-free Near-field Spectroscopy. *Appl. Phys. Lett.* **2006**, *89*, 101124.
- (20) García-Etxarri, A.; Romero, I.; García de Abajo, F. J.; Hillenbrand, R.; Aizpurua, J. Influence of the Tip in Near-field Imaging of Nanoparticle Plasmonic Modes: Weak and Strong Coupling Regimes. *Phys. Rev. B: Condens. Matter Mater. Phys.* **2009**, *79*, 125439.
- (21) Barth, A. Infrared Spectroscopy of Proteins. *Biochim. Biophys. Acta, Bioenerg.* **2007**, *1767*, 1073–1101.
- (22) Torma, P.; Barnes, W. L. Strong coupling between surface plasmon polaritons and emitters: A review. *Rep. Prog. Phys.* **2015**, *78*, 013901.
- (23) Olmon, R. L.; Raschke, M. B. Antenna-load Interactions at Optical Frequencies: Impedance Matching to Quantum Systems. *Nanotechnology* **2012**, *23*, 444001.
- (24) Olmon, R. L.; Rang, M.; Krenz, P. M.; Lail, B. A.; Saraf, L. V.; Boreman, G. D.; Raschke, M. B. Determination of Electric-Field, Magnetic-Field, and Electric-Current Distributions of Infrared Optical Antennas: A Near-Field Optical Vector Network Analyzer. *Phys. Rev. Lett.* **2010**, *105*, 167403.
- (25) Yoo, D.; et al. High-Contrast Infrared Absorption Spectroscopy via Mass-Produced Coaxial Zero-Mode Resonators with Sub-10 nm Gaps. *Nano Lett.* **2018**, *18*, 1930–1936.
- (26) O'Callahan, B. T.; Lewis, W. E.; Möbius, S.; Stanley, J. C.; Muller, E. A.; Raschke, M. B. Broadband Infrared Vibrational Nanospectroscopy Using Thermal Blackbody Radiation. *Opt. Express* **2015**, *23*, 32063–32074.